Evaluation of the potential of the current and forthcoming multispectral and hyperspectral imagers to estimate soil texture and organic carbon

Castaldi Fabio[1], Palombo Angelo[2], Santini Federico[2], Pascucci Simone[2], Pignatti Stefano[2], Casa Raffaele[1]

[1] *Department of Agricultural and Forestry scieNcEs (DAFNE), Università degli Studi della Tuscia, Via San Camillo de Lellis, 01100 Viterbo, Italy.*

[2]*Consiglio Nazionale delle Ricerche- Institute of Methodologies for Environmental Analysis (C.N.R. – IMAA), Via del Fosso del Cavaliere, 100, 00133 Roma, Italy.*

Correspondence: F.Castaldi, castaldi@unitus.it

Abstract

In this study the capabilities of seven multispectral and hyperspectral satellite imagers to estimate soil variables (clay, sand, silt and organic carbon content) were investigated using data from soil spectral libraries. Four current (EO-1 ALI and Hyperion, Landsat 8 OLI, Sentinel-2 MSI) and three forthcoming (EnMAP, PRISMA and HyspIRI) satellite imagers were compared. To this aim, two soil spectra datasets that simulated each imager were obtained: (*i*) resampled spectra according to the specific spectral response and resolution of each satellite imager and (*ii*) resampled spectra with declared or actual noise (radiometric and atmospheric) added. Compared with those using full spectral resolution data, the accuracy of Partial Least Square Regression (PLSR) predictive models generally decreased when using resampled spectra. In the absence of noise, the performances of hyperspectral imagers, in terms of Ratio of Performance to Interquartile Range (RPIQ), were generally significantly better than those of multispectral imagers. For instance the best RPIQ for sand estimation was obtained using EnMAP simulated data (2.56), whereas the outcomes gained using multispectral imagers varied from 1.56 and 2.28. The addition of noise to the simulated spectra brought about a decrease of statistical accuracy in all estimation models, especially for

Hyperion data. Although the addition of noise reduced the performance differences between multispectral and hyperspectral imagers, the forthcoming hyperspectral imagers nonetheless provided the best RPIQ values for clay (2.16–2.33), sand (2.10–2.17), silt (2.77–2.85) and organic carbon (2.48–2.51) estimation. To better understand the impact of spectral resolution and signal to noise ratio (SNR) on the estimation of soil variables, PLSR models were applied to resampled and simulated spectra, iteratively increasing the bandwidth to: 10, 20, 40, 80 and 160 nm. Results showed that, for a bandwidth of 40 nm, i.e., a spectral resolution lower than that of current and forthcoming imagers, the estimation accuracy was very similar to that obtained with a higher spectral resolution.

Forthcoming hyperspectral imagers will therefore improve the accuracy of soil variables estimation from bare soil imagery with respect to the results achievable by current hyperspectral and multispectral imagers. This work provides useful indications for the future application of satellite data in Soil Science, and for the estimation of the most important soil variables by next generation satellite imagers.

Keywords: *imaging spectroscopy, sand, clay, spectral library, SNR, PLSR, PRISMA, EnMAP, HyspIRI*

1. Introduction

Understanding variability of soil properties between and within agricultural fields allows for more efficient use of resources, improving agronomic and environmental management. The qualitative information included in existing soil maps is often insufficient for site-specific management strategies concerning water, fertilizers, herbicides or harvest. For these purposes, the quantitative estimation of soil properties (e.g., soil texture, organic carbon, nitrogen, and soil moisture) over the field is necessary. With the exception of a few regions in highly developed agricultural environments, this kind of information is rarely available to land managers.

Remote sensing data can be used to obtain, in a very cost effective way, qualitative and quantitative information about soil variables and soil classification (Mulder et al., 2011). In cultivated soils, due to repeated tillage operations, soil properties are usually quite uniform over the tilled layer; therefore they can be estimated from the bare soil surface reflectance (Casa et al., 2013b).

Quantitative estimation of soil variables using bare soil imagery acquired from multispectral remote imagers is, however, hampered by inadequate spectral resolution, particularly by the absence of narrow bands in the short wave infra-red (SWIR) region (1100–2400 nm) (i.e., the spectral region more affected by the soil chromophores). For these reasons, multispectral satellite data are mainly used for qualitative assessments, such as the classification of areas with different soil textures (e.g., Demattê et al., 2009; Odeh & McBratney, 2000; Zhai et al., 2006). Recent studies obtained a sufficient degree of accuracy in the quantitative estimation of silt (Wu et al., 2015) or clay (Castaldi et al., 2014) using, respectively, BJ-1 and Advanced Land Imager (ALI) satellite imagers. It should be noted that both the multispectral ALI imager on board the NASA EO-1 satellite and the Operational Land Imager (OLI) imager on board the Landsat 8 satellite, have bands in the SWIR region, which can be exploited for soil properties estimation. Sentinel-2, which was successfully launched in June 2015, has a Multispectral Imager (MSI) with a band in the SWIR region, between 2100 and 2280 nm and centred at 2190 nm, with a Ground Sampling Distance (GSD) of 20 m.

Hyperspectral imagers, that measure spectral radiance for hundreds of narrow bands are more attractive than multispectral imagers for soil spectroscopy purposes. Furthermore, over the last decade, analysis of data obtained by optical remote sensing techniques such as soil spectroscopy and hyperspectral imagery has proven to be an effective way to characterize and monitor surface soil variables, that even allow soil erosion processes to be detected (Gomez et al., 2015; Stevens et al., 2013; Ben-Dor et al., 2009; Lagacherie et al., 2008; Gomez, et al., 2008). The higher spectral resolution provided by hyperspectral sensors could, in principle, allow even more accurate quantitative estimates at the field scale, compared with those obtainable from the existing multispectral imagers (Mulder et al., 2011).

Only two hyperspectral satellite imagers with a sufficient spatial resolution (i.e., GSD ≤ 30 m) are currently available for soil applications: Hyperion on board of the NASA EO-1 platform and Compact High Resolution Imaging Spectrometer (CHRIS) on the European Space Agency's PROBA platform. Both these sensors have considerable limitations in quantitative soil estimation applications. Hyperion’s data are hampered by the very low signal to noise ratio (SNR) in the SWIR region, in particular around 2200 nm, where the spectral features of clay minerals are located (Castaldi et al., 2014). The difficulties in estimating soil variables from CHRIS-PROBA are due to its restricted spectral range (415–1050 nm) that lacks bands in the SWIR region (Casa et al., 2013a). For these reasons, the use of satellite hyperspectral data in quantitative soil estimation is still challenging and consequently the number of published studies in which this type of data are used is still small (Casa et al., 2013a; Casa et al., 2013b; Castaldi et al., 2014; Gomez et al., 2008; Zhang et al., 2013).

In the near future at least four satellites equipped with hyperspectral imagers are due to be launched: the Japanese Hyperspectral Imager Suite (HISUI) in 2017 (Tanii et al., 2012); the Italian PRecursore IperSpettrale della Missione Applicativa (PRISMA) in 2017 (Pignatti et al., 2012); the German Environmental Mapping and Analysis Program (EnMap) in 2018 (Richter et al. 2012); the China Commercial Remote-sensing Satellite System (CCRSS) after 2018; and the U.S. NASA Hyperspectral Infrared Imager (HyspIRI) in 2021 (Houborg et al. 2012). The Spaceborn Hyperspectral Applicative Land and Ocean Mission (SHALOM) — a joint mission by the Israel Space Agency (ISA) and the Italian Space Agency (ASI) — will also develop a hyperspectral imager with 241 bands between 400 and 2500 nm and a spectral resolution of about 10 nm (Ben-Dor et al., 2013). A new hyperspectral imager, HYPerspectral X Imagery (HYPXIM) is also under study by the French space agency (CNES) (Michel et al., 2011). Forthcoming hyperspectral imagers will have numerous narrow bands in the SWIR spectral region, which will presumably permit accurate estimation of soil variables; however, the soil properties estimation accuracy of these imagers will depend on their SNR, particularly around 2200 nm. Hyperspectral imagers generally have a lower SNR than multispectral ones as a result of the reduced energy collected by the sensor in narrow spectral bands. This effect, coupled with the low solar irradiance in the SWIR region, produces a consistent decrease of the SNR. For example, Castaldi et al. (2014) compared the soil estimation capabilities of two sensors mounted on EO-1 satellite using both Hyperion and ALI data. The authors did not observe any apparent advantages when using hyperspectral (Hyperion) instead of multispectral (ALI) data. This was explained by the low SNR of Hyperion at the wavelengths of characteristic spectral features of clay minerals.

This study aims to evaluate the performances of current and forthcoming multispectral and hyperspectral imagers for the quantitative retrieval of soil texture and Soil Organic Carbon (SOC). To this end we compare the estimation accuracy for soil texture (clay, sand and silt) and SOC using spectra acquired under laboratory conditions, which were resampled according to spectral and noise characteristics of four current (ALI, Landsat 8, Sentinel-2 and Hyperion) and three forthcoming (EnMAP, PRISMA, HyspIRI) satellite imagers. To our knowledge, no previous reports have specifically compared the capability of these imagers for soil texture and SOC estimation.

2. Materials and Methods

2.1. Soil spectral libraries

2.1.1. PONMAC library

A soil spectral library consisting of 166 samples was assembled by pooling together data from soil samplings carried out in two cropland areas in Central and Southern Italy. Samplings were carried out in Pontecagnano (PON; Southern Italy, near to Salerno) and Maccarese (MAC; Central Italy, near to Rome) and a pooled dataset obtained from the union of PON (Pascucci et al., 2014) and MAC (Casa et al., 2013b), hereafter referred to as PONMAC. The soils of the MAC area are classified as Cutanic Luvisol (FAO-ISRIC-ISSS, 1998), with soil parent materials of flat inshore deposits (Pleistocene), while the soils of PON area originated from travertine sediments characterized by sandy gravel layers with tuffaceous intercalation in the upper parts (Pleistocene–Holocene). In both areas, soil sampling was carried out using a gouge auger at 0–10 cm depth in Pontecagnano and at 0–30 cm depth in Maccarese. Soil samples were air dried and passed through a 2 mm sieve. For each sample we measured the percentage of clay, sand and silt contents using the pipette method according to the United States Department of Agriculture (USDA) system (Soil Survey Staff, 2014). Soil Organic Content (%) was obtained using the Walkley-Black method for PON data and an elemental analyzer (Flash EA1112, Thermo Electron Corporation, U.S.A.) according to the technique of dry combustion analysis (ISO 10694, 1995) for MAC data. Although SOC measurements were carried out using different methods for MAC and PON dataset, the results obtained from Walkley-Black and dry combustion analysis were considered to be comparable within the range of SOC values of the PONMAC dataset (Chen et al., 2015).

Soil textures of PONMAC samples are mainly composed of sandy clay loam, clay loam and clay. These textural classes are among the most frequent in the croplands of Italy (Costantini et al., 2012). The ranges of the relative contents (%) of clay, sand and silt in the PONMAC dataset are quite wide (Table 1). The SOC content range is between 0.5 and 2.32%, with a mean value of 1.25% (Table 1).

Soil samples were placed in Petri dishes and their spectral signatures were measured in a dark lab in the visible-near infrared (VNIR) to SWIR optical domain (350-2500 nm, spectral sampling of 1 nm) using an Analytical Spectral Devices (ASD) Field Spec Fr Pro spectroradiometer (ASD Inc., Boulder, CO, USA; available at: http://www.asdi.com) equipped with a contact probe containing a 7 W quartz-halogen lamp. Reflectance values from 350 to 399 nm and from 2401 and 2500 nm were removed prior to any processing because these spectral ranges are affected by noise.

The ASD measurements consisted of three spectral acquisitions at nadir rotating the sample by 90° each time. Each replicate involved 50 spectral scans and after every set of 50, a Spectralon panel (Labsphere, NH, USA) was measured before the sample was rotated. The average measured radiance was then converted into bi-conical reflectance using the calibrated Spectralon panel.

2.1.2. LUCAS library

In the framework of European Land/Use Cover Area frame Statistical Survey (LUCAS) about 20,000 topsoil samples were collected across Europe (Eurostat, 2009; Tóth et al., 2013). The soil properties of the LUCAS dataset were analyzed using ISO standards methods. The determination of particle size distribution was carried out using the sieving and sedimentation method (ISO 11277. 1998), and SOC was estimated by dry combustion using an elemental analyzer (ISO 10694:1995). Spectra were acquired on diffuse high-resolution reflectance for all air-dried and sieved (< 2 mm) soil samples using an XDS Rapid Content Analyzer (FOSS NIRSystems Inc,, Laurel, MD, USA) spectroscope, measuring a continuous (spectral resolution of 0.5 nm) reflectance spectrum in the VNIR (400–1300 nm) and SWIR (1300–2500 nm) domains. Soil spectroscopy measurements were made following the protocol of the Soil Spectroscopy Group (SPS, 2011).

In order to have a dataset comparable with PONMAC, we extracted from the LUCAS topsoil dataset only the samples collected on cropland areas in Italy (LUCAS_C) and we resampled the LUCAS spectra according to the spectral resolution of the PONMAC library (1 nm). The 713 samples thus extracted from the European LUCAS library are representative of all the soil regions in the Soil Map of Italy (Costantini et al., 2012) and display a large variability in clay, sand, silt and SOC contents (Table 1).

The PONMAC and LUCAS_C datasets cannot be fused into a single dataset however because different spectral acquisition techniques and protocols were used to measure reflectance.

2.2. Satellite sensors

The performances of seven satellite imagers were compared. We took into consideration three operating multispectral imagers (EO-1 ALI, Sentinel-2 MSI and LANDSAT 8 OLI), one operating hyperspectral imager (EO-1 Hyperion) and three forthcoming hyperspectral imagers (EnMAP, PRISMA and HyspIRI). The main technical specifications of the multispectral and hyperspectral imagers are summarized, respectively, in Table 2 and Table 3. In particular, the last two columns of both tables show the SNR at different wavelengths and the related signal intensities (Pignatti et al., 2013; Baillarin et al., 2012; Markham et al. 2012; Sang et al., 2008; Green et al., 2008; Mendenhall et al., 2001; Willoughby et al., 1996).

2.3. Resampled and simulated data

The LUCAS_C and PONMAC spectral libraries were used to produce two sets of synthetic spectra. A first set of spectra was obtained by resampling the library spectra, using convolution procedures, to the specific spectral response and resolution of the various sensors. This process was carried out using the spectral response function for the multispectral imagers, while for hyperspectral imagers the spectral response functions were not available and were subsequently approximated using Gaussian functions. The spectra obtained in this way are hereafter referred to as "resampled spectra".

In order to simulate the satellite data more realistically, an additional set of data was obtained by adding spectral noise to the synthetic spectra previously generated. For this purpose, we firstly applied a direct process that allowed us to simulate the spectral top of the atmosphere (TOA) at-sensor radiance, under specific illumination and acquisition geometries. The direct process can be represented by the equation (Vermote et al., 1997; Kaufmann et al., 1997):

$$L = \frac{A\rho}{1-\rho S} + L_a \qquad [1]$$

where L is the at-sensor radiance, L_a is the solar radiation scattered back to the sensor without reaching the soil (path radiance), ρ is the target reflectance, A is a parameter depending on the atmosphere alone (not on the illumination and acquisition geometries), and S is the spherical albedo of the atmosphere. In our simulations ρ was taken from the spectral libraries used for this study, while A, S and L_a were simulated by MODTRAN 4 code, using a standard midlatitude summer model to characterize the atmospheric column. The illumination geometry corresponds to the geographic coordinates of the center of Rome (41°53'35.94"N; 12°28'58.57"E) on the summer solstice at noon, local time. Once obtained, a spectral noise, consistent with the sensor radiometric characteristics and acquisition parameters, was added to the at-sensor TOA radiances.

In order to properly represent the noise dependence from the spectral radiance intensity reaching the sensor, more information than that shown in Tables 2 and 3 is needed. For HyspIRI and for all the multispectral imagers, with the exception of Sentinel-2, we found in the literature the spectral SNR at different radiance magnitudes. Since the covered intensity range was sufficiently wide, we could interpolate the SNR, thus obtaining look-up tables to identify the at-sensor spectral SNR at any radiance intensity. To fill in the missing information, we approached the research and technical teams of PRISMA and EnMAP for the spectral SNR at four different radiance levels, and were provided spectral information analogous to that already published for HyspIRI shown in Figure 1 (Green et al., 2008). Instead, for Hyperion and Sentinel-2 we were only able to obtain a unique spectral SNR level of a reference radiance, therefore we used a generic noise model to extrapolate the SNR at other radiance intensities (Chang, 2007):

$$SNR = SNR_{ref}\sqrt{\frac{L}{L_{ref}}} \qquad [2]$$

where, SNR_{ref} and L_{ref} are the nominal SNR and the related incident radiance, respectively. In this way, we managed to extrapolate the proper SNR at different illumination geometries and intensities.

After the conversion of the SNR to Noise equivalent in ΔRadiance (NeΔR), the noise to be added to Equation (3) was computed by applying Gaussian statistics. By using the described direct process (i.e., Equation (1)), we simulated the TOA radiance spectra (noise included) that each sensor would acquire for a set of different targets (reflectance spectra) at a specific time and day of the year.

Finally, the inverted process allowed us to calculate the top of the canopy (TOC) reflectance spectra as shown in Equation (3).

$$\rho = \frac{1}{A}[L - L_a - Gauss(0, Ne\Delta R)](1 - \rho S) \qquad [3]$$

In this way, for each original reflectance spectrum, we obtained a set of spectra consistent with the spectral and radiometric characteristics of the different analyzed satellite imagers. In other words, we simulated the spectra that would be obtained by the remote imagers after the application of radiometric and atmospheric corrections under a given illumination condition. These spectra are used to evaluate the potentials of the various imagers in the estimation of soil variables and are hereafter referred to as "simulated spectra". Figure 2 displays two Hyperion simulated reflectance spectra with (dashed line) and without (solid line) noise as obtained using a spectrum belonging to the PONMAC spectral library.

In order to investigate the issue of the low SNR of hyperspectral sensors, due to the reduced energy collected by the sensors in narrow spectral bands, the effect of broadening the bandwidths on the estimation accuracy of soil variables was examined. Synthetic (both resampled and simulated) spectra were iteratively resampled, doubling the bandwidth at each step. In Figure 3 five spectra obtained by resampling a simulated HyspIRI spectrum (PONMAC library) are depicted with five different bandwidths: 10, 20, 40, 80, and 160 nm. From Figure 3 it is evident that the bandwidth increase determines the progressive smoothing of some spectral features.

2.4. Soil variables estimation

We applied the Partial Least Square Regression (PLSR) technique (Wold et al., 2001) to estimate soil variables from three types of data: (*i*) full laboratory spectra (400–2400 nm; spectral resolution 1 nm); (*ii*) resampled spectra according to bands and spectral resolution of each satellite's imager; (*iii*) simulated spectra that were obtained by adding declared or actual sensors' noise, as well as atmospheric effects, to the resampled spectra.

In order to detect outliers, we used lower and upper limits of the distribution of each variable. Limits were set at 1.5 times the inter-quartile range (IQ) and observations outside the upper and lower value were considered outliers and eliminated from the following computations (Tukey, 1977). The IQ is the difference between the values below which 75% (Q3) and 25% (Q1) of the samples occur (IQ = Q3 − Q1). The number of samples removed as a result of this process is reported in Table 1. Moreover, skewed data (skewness >|0.5|) were transformed using the square root or logarithm of the variable (Table 1) to approximate a Gaussian distribution.

Before applying the PLSR method to the simulated spectra, the noisy bands falling into the absorption ranges of the atmospheric gases were removed. In Table 4 the removed spectral bands for each sensor are shown.

The PLSR is a multivariate regression technique widely used in soil spectroscopy applications. PLSR provides an optimal linear model that allows for the reduction of the number of correlated predictors (spectral bands) and transforms them to a restricted number of uncorrelated components (PLSR components), which have the best relationship with the dependent variables (in this case clay, sand, silt and SOC). In order to detect the main spectral regions that affect soil variables estimation, we calculated the variance importance in projection (VIP) values. The VIP value is a weighted sum of squares of the PLS weights. Weights are calculated from the amount of variance of dependent variables of each PLS component employed in the model (Wold et al., 2001). Predictors with VIP values greater than one are considered significant for the PLSR models because the average of VIP scores is equal to one (Chong & Jun, 2005).

Different PLSR models were preliminarily tested, using different combinations of PLSR components, spectral transformations and smoothing to obtain the most accurate prediction of soil variables in terms of root mean square error (RMSE). For these purposes the spectra were converted into absorbance (A) and/or first derivative (D) and the Savitzky-Golay (SG) smoothing filter was applied. The Savitzky-Golay filtering performs noise reduction and enhances small spectral differences; whereas derivative transformation of the spectra is useful for separating out peaks of overlapping bands and to reduce noise.

Each dataset was randomly split into calibration and validation subsets: 70% for calibration and 30% for validation subset, according to a modified multiple jack-knifing approach (Casa et al., 2013a; Bishop & McBratney, 2001). The splitting was repeated 100 times, quantifying the validation accuracy every time. The accuracy of the predictive models was finally evaluated by examining the coefficient of determination (R^2), RMSE (Eq. (4)), Ratio of the Performance to Deviation (RPD; Eq. (5)), and Ratio of Performance to Interquartile Range (RPIQ; Eq. (6)).The equations used were as follows:

$$RMSE = \sqrt{\frac{\sum_{i=1}^{n}(y_o - y_p)^2}{n}} \qquad [4]$$

$$RPD = \frac{sd}{RMSE} \qquad [5]$$

$$RPIQ = \frac{IQ}{RMSE} \qquad [6]$$

where, y_o and y_p are the observed and predicted values, respectively, n is the number of data pairs, and *sd* is the standard deviation of the observed values. We adopted threshold values of RPD usually employed in the soil spectroscopy literature to assess the accuracy of soil prediction models (Chang et al., 2001). These consider models with an excellent prediction capability to have RPD values of >2, intermediate capability to have values of 2–1.4 and unreliable model to have values of <1.4. Recently, Bellon-Maurel et al. (2010) warned of the reliability of these RPD thresholds because they were not statistically determined and the standard deviation, used in the numerator of the RPD equation, does not describe the correct range of variation for data with a skewed (non-normal) distribution. The RPIQ (using the IQ instead of *sd*) provides a more robust statistic to describe the performance of estimation models. For these reasons, both RPD and RPIQ values were reported to evaluate the capability of the prediction models.

The one hundred RPIQ validation values of each PLSR model were used to detect statistical differences among the estimation accuracies of the satellite imagers and between multispectral and hyperspectral imagers for each soil variable. A one-way analysis of variance (ANOVA) was applied to the RPIQ values of the one hundred replicates in order to verify that the differences between RPIQ means were statistically significant ($P < 0.01$). Fisher's Least Significant Difference (LSD) test was then applied to evaluate the statistical differences. The results of the significance test for RPIQ can be considered equivalent to those that could be obtained by testing differences in RMSE because of the relationship between the two statistics (Eq.6).

The PLSR analyses were performed using the pls (Mevik et al., 2013) packages developed in R software (R Development Core Team, 2011).

3. Results

3.1. Soil variables estimation using full spectra

The estimation of soil variables using the PONMAC full-resolution spectral library provided good results: all soil texture variables were predicted with a RMSE lower than 5.4%, RPD near to 2 and RPIQ of 2.51 for sand and higher than 3 for clay and silt (Table 5).

The statistical accuracy obtained using the LUCAS_C full-resolution spectral library was lower compared with that obtained using the PONMAC library for all soil variables (Table 6). In this case only the clay estimation model provided satisfactory prediction accuracy (Table 6; RMSE = 7.63; RPD = 1.69; RPIQ = 2.34; R^2 = 0.64).

The VIP analysis highlighted the most important spectral regions for PLSR models of each variable (Fig. 4). Clay, sand, silt and SOC estimation are highly affected by the wavelength range between 1900 and 2400 nm (VIP>1), but VIP values >1 are also present in the VIS region between 400 and 600 nm.

3.2. Soil variables estimation using resampled spectra

Compared with the full spectra PONMAC dataset, the accuracy of predictive models generally decreased when using resampled spectra both for hyperspectral and multispectral imagers, especially in the case of clay and silt estimation (Table 5). The RPIQ values obtained from full spectrum data for clay (RPIQ = 3.07) and silt (RPIQ = 3.17) estimation were significantly higher than those obtained with resampled spectra (Table 5), while no significant differences were observed between full spectrum (RPIQ = 2.51) and all hyperspectral imagers

(RPIQ ranges from 2.45 and 2.56) for sand. The estimation accuracy of SOC for full spectrum (RPIQ = 3.12), EnMAP (RPIQ = 3.11) and PRISMA (RPIQ = 3.02) data is statistically higher as compared with the other imagers.

As expected, in the absence of noise, and taking into consideration only the spectral characteristics (number, width and distribution of bands), the performances of the forthcoming hyperspectral imagers are significantly better than those of multispectral imagers and are very similar to Hyperion for all soil variables. An exception is observed for clay estimation with Sentinel-2 data that showed results (RPIQ = 2.54) very similar to those achieved using PRISMA and HyspIRI data (RPIQ = 2.43), while for sand, silt and SOC, the differences with respect to hyperspectral imagers were statistically significant. Sentinel-2 data showed the best performances among multispectral imagers for all variables, except for silt (Table 5).

In the case of the LUCAS_C spectral library, differences between full-resolution and resampled dataset were not always significantly in favor of hyperspectral sensors. The LSD test highlighted an advantage of using simulated data instead of full spectrum data for the estimation of soil texture components (Table 6). For example, the resampled hyperspectral data (HyspIRI, EnMAP and PRISMA) showed significantly better results (RPIQ: 1.84–1.87) compared with full spectrum data (RPIQ: 1.74) for silt estimation. Otherwise, a substantial decrease of accuracy (compared with full spectra) is observed only for multispectral data (Table 6) with the exception of silt estimation, for which the accuracy obtained by full spectrum data was not statistically different from that obtained with ALI and Sentinel-2 data (RPIQ: 1.71–1.76).

3.3. Soil variables estimation using simulated spectra

The use of simulated spectra, i.e. with the addition of noise and atmospheric effects, resulted in a decrease of statistical accuracy in the estimation models, compared with full or resampled spectra, both using PONMAC and LUCAS_C spectral libraries. Hyperion simulated data appear particularly affected by noise, showing RPIQ values similar or lower than those achieved using multispectral data (Table 7). Indeed, the LSD test carried out on the validation statistics of the PONMAC dataset showed that the simulated Hyperion data provided similar or worse results than multispectral imagers (Table 7). For clay estimation the best RPIQ values were obtained using EnMAP, PRISMA and HyspIRI data (PONMAC: 2.16–2.35; LUCAS_C: 1.95–2.00). The forthcoming hyperspectral imagers (EnMAP, PRISMA and HyspIRI) display very similar capability levels when estimating soil texture and SOC content both for the PONMAC (Table 7) and LUCAS_C (Table 8) dataset. Only clay content was estimated with a suitable level of accuracy using PRISMA and HyspIRI resampled spectra of LUCAS_C dataset (Table 8).

The difference in statistical accuracy between hyperspectral and multispectral data becomes less consistent when using simulated data compared with resampled data. In many cases multispectral data have similar or better results than hyperspectral, for example Landsat 8 provided an estimation accuracy of SOC estimation (RMSE = 0.25; RPD = 1.44; RPIQ = 2.48; R^2 = 0.49) not statistically different to hyperspectral imagers using PONMAC dataset. Satisfactory estimation accuracy was also achieved by ALI when estimating clay (RPD = 1.45; RMSE = 6.58) and for all the multispectral imagers when estimating silt using PONMAC dataset. However, for each soil variable, the LSD test confirmed better estimation accuracy of the forthcoming hyperspectral imagers than for the current multispectral imagers.

3.4. Sensitivity to bandwidth of the estimation models

The issue of the low SNR of hyperspectral sensors due to the reduced energy collected by the sensors in narrow spectral bands (evidenced by the results of the previous section) was investigated by examining the effect of broadening the bandwidths. The application of PLSR models to the PONMAC datasets showed, for all variables only a slight decrease of estimation accuracy when changing bandwidth from 10 to 40 nm (Fig. 5) in the case of absence of noise (resampled dataset). A greater decrease of the RPD values is observed when using a bandwidth greater than 80 nm. After the introduction of noise (simulated dataset), the SOC estimation accuracy is almost insensitive to the reduction of spectral resolution, while RPD values of clay and sand even increase slightly up to 40 nm (Fig. 6). Furthermore, the RPD values only decrease significantly when using a bandwidth greater than 80 nm.

4. Discussion

The statistical accuracy obtained using the LUCAS_C spectral library was generally lower than that obtained with the PONMAC dataset for full spectrum, resampled and simulated data. These differences in model accuracy are probably due to the high variability of the LUCAS_C dataset (Table 1), and to the different methodologies adopted for soil analyses and spectra acquisition. Although soil samples of the PONMAC dataset cover a wide range of clay, sand, silt and SOC values they are characterized by two types of parental material. On the other hand, LUCAS_C represents most of the agricultural soils of Italy. This high variability includes different compositions of clay minerals and organic matter among soil samples, which influences the number and diversity of PLSR components. In this regard, the typical absorption features related to the clay lattice are different according to the predominant clay mineral: the absorption features of kaolinite and montmorillonite are located at 1400, 1900, and 2200 nm (Clark, 1999), whereas illite has two bands around 2300 and 2400 nm. The typical absorption features of organic matter are distributed throughout the entire reflectance VNIR–SWIR spectrum. This is due to its heterogeneous composition, in turn derived from varied source materials and their mineralization levels (Ben-Dor et al., 1997; Li et al., 2012; Mouazen Maleki et al., 2007). Therefore, the heterogeneous composition of the soil samples of the LUCAS_C dataset involves the use of more PLSR components than those used for the PONMAC dataset (Table 5; Table 6).

The VIP analysis confirmed the most important spectral region (VIP>1) for clay, sand, silt and SOC is located between 1900 and 2400 nm. This result can be attributed mainly to the presence of typical absorption features in the SWIR spectral region. In particular, metal-OH bending and stretching of O-H bonds related to the clay lattice affect the absorption peaks between 2160 and 2300 nm (Ben-Dor et al., 2009); while VIP scores of SOC in the SWIR are mainly affected by phenolic, amide and aliphatic groups between 2200 and 2220 nm. The high VIP values around 1900 nm are due to the absorption features of water. Viscarra-Rossel and Beherens (2010) used VIP values to select the most useful bands for estimating clay and SOC by means of diffuse reflectance spectra. Most of the selected bands they identified, for both variables, were located between 1900 and 2400 nm, similarly to our results.

VIP values greater than 1 are present also in the VIS region between 400 and 600 nm. Viscarra-Rossel et al. (2008) detected high VIP values between 400 and 600 nm for SOC estimation, using spectra acquired by an infrared spectrometer from 400 to 1000 nm. Although some wavelengths correlated with organic matter exist at 450 nm and 590 nm (Melendez-Pastor et al., 2008; Li et al., 2012), the main information provided by the VIS region, for texture and SOC estimation, is likely to be related to the hue of soil. Since soils having dark hues, for equal moisture content and parental material, generally contain higher clay and SOC and lower sand content than soils with pale hues. The consistent worsening of the estimation accuracy when using simulated hyperspectral data, instead of resampled spectra, highlights the importance of the effect of the noise affecting the various instruments. In general the noise particularly affects the SWIR region, especially from 2000 nm to 2400 nm (Fig. 1 and Fig. 2), where the VIP analysis provided the higher values (Fig. 4). In addition, the very low SNR that corresponds to water absorption features required the elimination of the corresponding spectral bands.

The estimation accuracy showed that the addition of noise to the spectra reduces the differences of performance between hyperspectral and multispectral imagers. However the LSD test detected a significant difference between hyperspectral (with exclusion of Hyperion) and multispectral imagers, for both spectral libraries and each soil variable. Furthermore, the accuracy of soil variable estimation is very similar for the three forthcoming imagers (Table 7 and Table 8), in spite of the fact that EnMAP and PRISMA present (in sensitive spectral ranges) a greater number of bands (but a lower SNR) than HyspIRI (Table 9). These results are explainable if the SNR, which generally decreases with the spectral resolution due to the lower energy reaching the sensors, partially compensates the benefits of the higher spectral resolution, thus better exploiting narrow spectral features. Obviously, spatial resolution influences, *ceteris paribus*, the prediction accuracy of soil variables (Gomez et al., 2015). For this reason, the estimation accuracy obtained by HyspIRI would not be perfectly comparable with EnMap and PRISMA data, because the US imager will have a spatial resolution much coarser (GSD of 60 m) than the other hyperspectral sensors investigated in this work (GSD of 30 m).

The analysis concerning the sensitivity to bandwidth of the estimation accuracy of soil variables showed that data acquired between 400 and 2400 nm, with a bandwidth of 40 nm could provide results very similar to those obtained using sensors with a higher spectral resolution, because of the lower SNR of the former. However, a bandwidth of 40 nm could be useful for multivariate prediction models, such as the PLSR, where the spectral information is summarized in a restricted number of regressors (PLSR components) correlated with the target variable. Actually, PLSR technique has proved less effective than other hybrid estimation techniques, such as regression kriging (Casa et al., 2013a) or linear mixed effect models (Castaldi et al., 2014); however these hybrid techniques cannot be used with laboratory samples because they take into account the spatial correlation between soil samples.

The higher spectral resolution of hyperspectral data permits exploitation of well-defined narrow absorption spectral features typically associated to overtones of functional groups in the VNIR and SWIR spectral ranges related to the estimation of some chromophores (Ben-Dor et al., 2009), such as the clay minerals (Clark, 1999). Unfortunately, the sensor's noise generally increases with increasing spectral resolution. Thus, as confirmed by the analysis of the sensitivity to bandwidth, the advantages of detecting specific narrow bands could be nullified by low SNR, especially in the SWIR spectral region where the absorption peaks of the main soil variables are located (Lobell & Asner, 2002).

This work provides an evaluation of the capability of the remote imagers to estimate soil variables using simulated spectra, taking into account the spectral resolution and noise of each imager and the atmospheric effect. Both PONMAC and LUCAS_C spectral libraries are composed by spectra acquired in laboratory conditions on air dried soil samples, having an artificial roughness; however the actual remote sensing data are also affected by the confounding effects of soil moisture, soil roughness and crop residues. Soil moisture has a strong influence on the amount and composition of reflected and emitted energy from a soil surface, reducing the reflectance over the entire spectrum (Lobell & Asner, 2002; Nocita et al., 2013; Rienzi et al. 2014; Castaldi et al. 2015), and the soil roughness influences the scattering effect. The drying process of soil samples of both datasets used in the present work has occurred naturally and for this reason soil datasets preserved moisture variability which could be assumed to be similar to that observable on the top layer of an agricultural soil, with quite a homogenous roughness, after a period of dry weather. In this regard there are many examples in the literature of the estimation of soil variables using remote data which assume the homogeneity of soil roughness of the bare soil after seed bed preparation, thus without crop residues or weeds within the field (Casa et al., 2013b; Ge et al., 2011; Mulder et al., 2011; Selige et al., 2006). Nevertheless, the capability of the present and forthcoming satellite imagers shall be assessed using actual data. Effective comparisons can only be done using satellite data acquired for a particular field site over a particular time period. In this regard, Castaldi et al. (2014) compared Hyperion and ALI imager using images acquired on the same date and obtained more accurate prediction with Hyperion as compared with ALI for clay, sand and soil organic matter. However, at present, the comparison among current and forthcoming sensors is only possible using spectral laboratory data covering the whole VIS–SWIR spectral range (e.g., PONMAC and LUCAS_C), considering that a satellite hyperspectral sensor having spectral characteristics suitable to simulate PRISMA, EnMAP or HyspIRI images does not exist yet.

5. Conclusions

This work investigates, for seven satellite imagers, the effects of spectral resolution and SNR on the estimation of some soil variables such as clay, sand, silt and SOC by using PLSR models. We compared the estimation accuracy of soil texture and SOC using resampled and simulated spectra according to spectral and noise characteristics of four current (ALI, Landsat 8, Sentinel-2 and Hyperion) and three forthcoming (EnMAP, PRISMA, HyspIRI) satellite imagers. The LSD testing on simulated data (Table 8) suggests that the forthcoming hyperspectral imagers will enhance, in relative terms, the accuracy of soil variable estimation from bare soil imagery, as compared to current generation sensors, though in absolute terms the statistics of their performance (e.g. in terms of r^2) was not always satisfactory. The advancement of the new generation hyperspectral imagers, as compared to Hyperion, is due to the improvement of the SNR in the SWIR region, in particular between 2000 and 2400 nm. EnMAP, PRISMA and HyspIRI imagers provided significantly better estimation accuracy than ALI, Landsat 8 and Sentinel-2. This is mainly due to the higher number of bands, especially in SWIR region, and the narrower bandwidths that allow them to better exploit the spectral features of clay minerals and organic matter. However, the benefit of improved spectral resolution is partially offset by the amplification of noise when increasing the number of spectral bands. Analysis of the sensitivity to bandwidth highlighted that a bandwidth of 40 nm could provide PLSR results very similar to those obtained with sensors having a higher spectral resolution and that, only when the noise levels are decreased, the capabilities of current and forthcoming hyperspectral sensors will be fully achieved. The analysis also indicates that 40 nm is a maximum value for the bandwidth, beyond which the estimation accuracy of soil texture sharply decreases.

We conclude that hyperspectral data from the forthcoming satellite missions could be more valuable for mapping and monitoring soil texture and SOC as compared to current imagers. The higher spectral resolution of the new imagers, coupled to an improved SNR and an extensive spatial coverage and frequent revisit period, will guarantee highly detailed spectral information, suitable to characterize and monitor surface soil variables and soil erosion processes. Nevertheless, as shown in this work, the achievement of satisfactory quantitative estimation results from hyperspectral imagers is still hampered by a low SNR in the SWIR spectral region, especially apparent when using a large and varied dataset (LUCAS_C). On the other hand, the use of hyperspectral data joined with spatial predictive models on delimitated field data (PONMAC) could lead to a satisfactory estimation of soil variables. [rc1]

Further research will need to focus on estimation accuracies for the retrieval of soil variables using, once available, real data from next generation hyperspectral satellite imagers.

Acknowledgements

The research activities have been co-funded by the Italian Space Agency (ASI) with grant I/019/11/10 (PRISMA Mission). Additionally, we would like to thank to the PRISMA, EnMAP and HyspIRI teams for having provided information on the radiometric characteristics of the sensors useful for the production of the datasets used in this paper. Additionally we are grateful to the anonymous reviewers for their valuable comments, which helped to improve the quality of this paper.

References

Baillarin, S.J., Meygret, A., Dechoz, C., Lacherade, S., Tremas, T., Isola, C., ... Spoto, F. (2012). Sentinel-2 level 1 products and image processing performances. Proceedings of Geoscience and Remote Sensing Symposium (IGARSS), 2012 IEEE International , pp.7003–006, 22–27 July 2012.

Bellon-Maurel, V., Fernandez-Ahumada, E., Palagos, B., Roger, J.M., & McBratney, A. (2010). Critical review of chemometric indicators commonly used for assessing the quality of the prediction of soil attributes by NIR spectroscopy. *TrAC Trends in Analytical Chemistry*, *29*(9), 1073–1081. doi:10.1016/j.trac.2010.05.006.

Ben-Dor, E., Inbar, Y., Chen, Y. (1997). The reflectance spectra of organic matter in the visible near-infrared and short wave infrared region (400–2500 nm) during a controlled decomposition process. *Remote Sensing of Environment*, *61*(1), 1–15. http://doi.org/10.1016/S0034-4257(96)00120-4

Ben-Dor, E., Chabrillat, S., Demattê, J.A.M., Taylor, G.R., Hill, J., Whiting, M.L., & Sommer, S. (2009). Using Imaging Spectroscopy to study soil properties. *Remote Sensing of Environment*, *113*, S38–S55. http://doi.org/10.1016/j.rse.2008.09.019

Ben-Dor, E., Kafri A., & Varacalli G. (2013). SHALOM: Spaceborne Hyperspectral Applicative Land and Ocean Mission: A joint project of ASI – ISA. Proceedings of the International Geoscience and Remote Sensing Symposium (IAGARSS'13), Melbourne, Australia, 4 pages, 2013.

Bishop, T.F., & McBratney, A. (2001). A comparison of prediction methods for the creation of field-extent soil property maps. *Geoderma*, *103*(1–2), 149–160. doi:10.1016/S0016-7061(01)00074-X

Casa, R., Castaldi, F., Pascucci, S., Basso, B., & Pignatti, S. (2013a). Geophysical and hyperspectral data fusion techniques for in-field estimation of soil properties. *Vadose Zone Journal*, *12*(4). doi:10.2136/vzj2012.0201

Casa, R., Castaldi, F., Pascucci, S., Palombo, A., & Pignatti, S. (2013b). A comparison of sensor resolution and calibration strategies for soil texture estimation from hyperspectral remote sensing. *Geoderma*, *197–198*, 17–26. doi:10.1016/j.geoderma.2012.12.016

Castaldi, F., Casa, R., Castrignanò, A., Pascucci, S., Palombo, A., & Pignatti, S. (2014). Estimation of soil properties at the field scale from satellite data: a comparison between spatial and non-spatial techniques. *European Journal of Soil Science*, *65*(6), 842–851. doi:10.1111/ejss.12202

Castaldi, F., Palombo, A., Pascucci, S., Pignatti, S., Santini, F., & Casa, R. (2015). Reducing the Influence of Soil Moisture on the Estimation of Clay from Hyperspectral Data: A Case Study Using Simulated PRISMA Data. Remote Sensing, 7(11), 15561–15582. doi:10.3390/rs71115561

Chang C. I. (2007). *Hyperspectral Data Exploitation: Theory and Applications.* Hoboken, NJ: Wiley.

Chang, C.W., Laird, D.A., Mausbach, M.J., & Hurburgh, C.R. (2001). Near-Infrared Reflectance Spectroscopy – Principal components regression analyses of soil properties. *Soil Science Society of America Journal*, *65*(2), 480. doi:10.2136/sssaj2001.652480x

Chen, L., Flynn, D.F.B., Jing, X., Kühn, P., Scholten, T., & He, J.S. (2015). A comparison of two methods for quantifying soil organic carbon of alpine grasslands on the Tibetan Plateau. *PLOS ONE*, *10*(5), e0126372. doi:10.1371/journal.pone.0126372

Chong, I.G., & Jun, C.H. (2005). Performance of some variable selection methods when multicollinearity is present. *Chemometrics and Intelligent Laboratory Systems*, *78*(1-2), 103–112

Clark, R.N. 1999. Chapter 1: Spectroscopy of Rocks and Minerals, and Principles of Spectroscopy, in: Rencz A.N. (Eds.*), Manual of Remote Sensing*, John Wiley and Sons, New York, pp 3- 58.

Costantini, E.A.C., L'Abate, G., Barbetti, R., Fantappié, M., Lorenzetti, R. and Magini, S. (2012). Carta dei suoli d'Italia, scala 1:1.000.000 (Soil map of Italy, scale 1:1.000.000).

Consiglio per ricerca e la sperimentazione in agricoltura, S.EL.CA. Florence/Firenze, Italy (ISBN: 978-88-97002-02-4). Available at: http://www.soilmaps.it/

Demattê, J.A.M., Fiorio, P.R., & Ben-Dor, E. (2009). Estimation of soil properties by orbital and laboratory reflectance means and its relation with soil classification. *The Open Remote Sensing Journal*, *2*(1), 12–23. doi:10.2174/1875413900902010012

FAO-ISRIC-ISSS. (1998). World Reference Base for Soil Resources. World Soil Resources Report 84. Food and Agriculture Organisation, Rome, Italy.

Ge, Y., Thomasson, J. A., & Sui, R. (2011). Remote sensing of soil properties in precision agriculture: A review. *Frontiers of Earth Science, 5*(3), 229 - 238. doi:10.1007/s11707-011-0175-0

Gomez, C., Oltra-Carrió, R., Bacha, S., Lagacherie, P., & Briottet, X. (2015). Evaluating the sensitivity of clay content prediction to atmospheric effects and degradation of image spatial resolution using Hyperspectral VNIR/SWIR imagery. *Remote Sensing of Environment*, *164*, 1–15. http://doi.org/10.1016/j.rse.2015.02.019

Gomez, C., Viscarra Rossel, R.A., & McBratney, A.B. (2008). Soil organic carbon prediction by hyperspectral remote sensing and field vis-NIR spectroscopy: An Australian case study. *Geoderma*, *146*(3-4), 403–411. doi:10.1016/j.geoderma.2008.06.011

Green, R.O., Asner, G., Ungar, S., & Knox, R. (2008). NASA mission to measure global plant physiology and functional types. Proceedings in Aerospace Conference, 2008 IEEE, pp.1–7, 1–8 March 2008. doi: 10.1109/AERO.2008.4526244

Houborg, R., Anderson, M., Gao, F., Schull, M., & Cammalleri, C. (2012). Monitoring water and carbon fluxes at fine spatial scales using HyspIRI-like measurements. In *2012 IEEE*

International Geoscience and Remote Sensing Symposium, pp. 7302–7305. IEEE. doi:10.1109/IGARSS.2012.6351975

International Standards Organisation 10694 (1995). Soil quality — Determination of organic and total carbon after dry combustion (elementary analysis)

International Standards Organisation 11277 (1998). Soil quality — Determination of particle size distribution in mineral soil material — Method by sieving and sedimentation.

Kaufmann, Y.J., Wald, A.E., Remer, L.A., Gao, B.C., Li, R.R., & Flynn, L. (1997). The MODIS 2.1-mm channel-correlation with visible reflectance for use in remote sensing of aerosol. Proceedings in IEEE Transactions on Geoscience and Remote Sensing. Vol. 35, no. 5, pp. 1286–1298.

Lagacherie, P., Baret, F., Feret, J.B., Netto, J.M., & Robbez-Masson, J.M. (2008). Estimation of soil clay and calcium carbonate using laboratory, field and airborne hyperspectral measurements, *Remote Sensing of Environment*, *112*, 825–835. doi:10.1016/j.rse.2007.06.014.

Li, D., Chen, X., Peng, Z., Chen, S., Chen, W., Han, L., & Li, Y. (2012). Prediction of soil organic matter content in a litchi orchard of South China using spectral indices. *Soil and Tillage Research*, *123*, 78–86. doi:10.1016/j.still.2012.03.013

Lobell, D.B., & Asner, G.P. (2002). Moisture effects on soil reflectance. *Soil Science Society of America Journal*, *66*(3), 722–727. Retrieved from http://www.scopus.com/inward/record.url?eid=2-s2.0-0036240171&partnerID=tZOtx3y1

Mulder, V.L., de Bruin, S., Schaepman, M.E., & Mayr, T.R. (2011). The use of remote sensing in soil and terrain mapping — A review. *Geoderma*, *162*(1-2), 1–19. doi:10.1016/j.geoderma.2010.12.018

Markham, B.L., Knight, E.J., Canova, B., Donley, E., Kvaran, G., Lee, K., Barsi, J.A., Pedelty, J.A., Dabney, P.W., & Irons, J.R. (2012). The Landsat data continuity mission Operational Land Imager (OLI) sensor. Proceedings in Geoscience and Remote Sensing Symposium (IGARSS), 2012 IEEE International, pp.6995–6998, 22–27 July 2012. doi: 10.1109/IGARSS.2012.6351961

Melendez-Pastor, I., Navarro-Pedreño, J., Gómez, I., & Koch, M. (2008). Identifying optimal spectral bands to assess soil properties with VNIR radiometry in semi-arid soils. *Geoderma*, *147*(3), 126–132.

Mendenhall, J.A., Hearn, D.R., Evans, J.B, Lencioni, D.E., Digenis, C.J., & Welsh, R.D. (2001) Initial flight test results from the EO-1 Advanced Land Imager: radiometric performance. Proceedings in Geoscience and Remote Sensing Symposium, 2001. IGARSS '01. IEEE 2001 International , vol.1, pp.515 -517, IEEE. doi: 10.1109/IGARSS.2001.976207

Mevik, B.H. & Wehrens, R. 2007. The pls package: Principal component and partial least squares regression in R. *Journal of Statistical Software*, *18,* 1–23.

Michel, S., Gamet, P., & Lefevre-Fonollosa, M.J. (2011). HYPXIM — A hyperspectral satellite defined for science, security and defence users. IEEE Proceedings in *2011 3rd Workshop on Hyperspectral Image and Signal Processing: Evolution in Remote Sensing (WHISPERS)* (pp. 1–4). doi:10.1109/WHISPERS.2011.6080864

Mouazen, A.M., Maleki, M.R., De Baerdemaeker, J., & Ramon, H. (2007). On-line measurement of some selected soil properties using a VIS–NIR sensor. *Soil and Tillage Research*, *93*(1), 13–27. doi:10.1016/j.still.2006.03.009.

Mulder, V.L., de Bruin, S., Schaepman, M.E., & Mayr, T. R. (2011). The use of remote sensing in soil and terrain mapping — A review. *Geoderma*, *162*(1-2), 1–19. doi:10.1016/j.geoderma.2010.12.018

Nocita, M., Stevens, A., Noon, C., & van Wesemael, B. (2013). Prediction of soil organic carbon for different levels of soil moisture using Vis-NIR spectroscopy. *Geoderma*, *199*, 37–42. http://doi.org/10.1016/j.geoderma.2012.07.020

Odeh, I.O., & McBratney, A.B. (2000). Using AVHRR images for spatial prediction of clay content in the lower Namoi Valley of eastern Australia. *Geoderma*, *97*(3–4), 237–254. doi:10.1016/S0016-7061(00)00041-0

Pascucci, S., Casa, R., Belviso, C., Palombo, A., Pignatti, S., & Castaldi, F. (2014). Estimation of soil organic carbon from airborne hyperspectral thermal infrared data: a case study. *European Journal of Soil Science*, *65*(6), 865–875. doi:10.1111/ejss.12203

Pignatti, S., Acito, N., Amato, U., Casa, R., de Bonis, R, Diani, M., … Cuomo, V. (2012). Development of algorithms and products for supporting the Italian hyperspectral PRISMA mission: The SAP4PRISMA project. Proceedings in *2012 IEEE International Geoscience and Remote Sensing Symposium* (pp. 127–130). IEEE. doi:10.1109/IGARSS.2012.6351620

Pignatti, S., Palombo, A., Pascucci, S., Romano F., Santini F., Simoniello T.,…Ananasso C. (2013). The PRISMA hyperspectral mission: Science activities and opportunities for agriculture and land monitoring. Proceedings *in Geoscience and Remote Sensing*

Symposium (IGARSS), 2013 IEEE International , pp.4558 -4561, 21-26 July 2013. doi: 10.1109/IGARSS.2013.6723850.

R Development Core Team 2011. R: A Language and Environment for Statistical Computing. R Foundation for Statistical Computing, Vienna. ISBN 3-900051-07-0 [WWW document]. Retrieved from: http://www. R-project.org/.

Richter, K., Hank, T., Atzberger, C., Locherer, M., & Mauser, W. (2012). Regularization strategies for agricultural monitoring: The EnMAP vegetation analyzer (AVA). Proceeedings in *2012 IEEE International Geoscience and Remote Sensing Symposium*, pp. 6613–6616. IEEE. doi:10.1109/IGARSS.2012.6352083

Rienzi, E.A., Mijatovic, B., Mueller, T.G., Matocha T.J., Sikora F.J., & Castrignanò A. (2014). Prediction of soil organic carbon under varying moisture levels using reflectance spectroscopy. *Soil Science Society of America Journal*, *78*(3), 958. http://doi.org/10.2136/sssaj2013.09.0408

Sang, B., Schubert, J., Kaiser, S., Mogulsky V., Neumann C., Förster K.P., … Chlebek C. (2008). The EnMAP hyperspectral imaging spectrometer:instrument concept, calibration and technologies. Proceedings in SPIE 7086, Imaging Spectrometry XIII, 708605 (27 August 2008). doi: 10.1117/12.794870

Selige, T., Böhner, J., & Schmidhalter, U. (2006). High resolution topsoil mapping using hyperspectral image and field data in multivariate regression modeling procedures. *Geoderma*, *136*(1–2), 235–244. doi:10.1016/j.geoderma.2006.03.050

Soil Survey Staff 2014. Keys to Soil Taxonomy, 12th edn. USDA-Natural Resources Conservation Service, Washington.

SPS (2011). The Soil Spectroscopy Group. Availble at: http://groups.google.com/group/soil-spectroscopy

Stevens, A., Nocita, M., Tóth, G., Montanarella, L., & van Wesemael, B. (2013). Prediction of soil organic carbon at the European scale by visible and near infrared reflectance spectroscopy, *PLoS ONE*, *8*(6), 1–13.

Tanii, J., Iwasaki, A., Kawashima, T., & Inada, H. (2012). Results of evaluation model of Hyperspectral Imager Suite (HISUI). Proceedings in *2012 IEEE International Geoscience and Remote Sensing Symposium*, pp. 131–134. IEEE. doi:10.1109/IGARSS.2012.6351619

Tóth, G., Jones, A., & Montanarella, L. (2013). The LUCAS topsoil database and derived information on the regional variability of cropland topsoil properties in the European Union. *Environmental Monitoring and Assessment*, *185*(9), 7409–25. doi:10.1007/s10661-013-3109-3

Tukey, J. W. (1977). Some thoughts on clinical trials, especially problems of multiplicity. *Science*, *198*(4318), 679–684. Retrieved from http://www.scopus.com/inward/record.url?eid=2-s2.0-0017778629&partnerID=tZOtx3y1

Vermote, E.F., Tanre, D., Deuze, J.L., Herman, M., & Morcette, J.J. (1997). Second simulation of the satellite signal in the solar spectrum, 6S: an overview. *IEEE Transactions on Geoscience and Remote Sensing*, 35(3), 675–686. doi:10.1109/36.581987

Viscarra Rossel, R. A., & Behrens, T. (2010). Using data mining to model and interpret soil diffuse reflectance spectra. *Geoderma*, 158(1-2), 46–54. doi:10.1016/j.geoderma.2009.12.025

Viscarra Rossel, R. A., Fouad, Y., & Walter, C. (2008). Using a digital camera to measure soil organic carbon and iron contents. *Biosystems Engineering*, 100(2), 149–159. doi:10.1016/j.biosystemseng.2008.02.007

Willoughby, C.T., Marmo, J., & Folkman, M.A. (1996). Hyperspectral imaging payload for the NASA small satellite technology initiative program, Proceedings in Aerospace Applications Conference, vol.2, pp.67–79. IEEE. doi: 10.1109/AERO.1996.495966

Wold, S., Sjöström, M., & Eriksson, L. (2001). PLS-regression: a basic tool of chemometrics. *Chemometrics and Intelligent Laboratory Systems*, *58*(2), 109–130. Retrieved from http://www.sciencedirect.com/science/article/pii/S0169743901001551

Wu, J., Li, Z., Gao, Z., Wang, B., Bai, L., Sun, B., … Ding, X. (2015). Degraded land detection by soil particle composition derived from multispectral remote sensing data in the Otindag Sandy Lands of China. *Geoderma*, *241-242*, 97–106. doi:10.1016/j.geoderma.2014.11.011

Zhai, Y., Thomasson, J.A., Boggess, J.E., & Sui, R. (2006). Soil texture classification with artificial neural networks operating on remote sensing data. *Computers and Electronics in Agriculture*, *54*(2), 53–68. doi:10.1016/j.compag.2006.08.001

Zhang, T., Li, L., & Zheng, B. (2013). Estimation of agricultural soil properties with imaging and laboratory spectroscopy. *Journal of Applied Remote Sensing*, *7*(1), 073587. doi:10.1117/1.JRS.7.073587

Figure captions

Figure 1. HyspIRI spectral noise characteristics provided by HyspIRI scientific team. The SNR spectra (left) are shown for four different radiance levels (right), corresponding to different albedo and solar zenith angles.

Figure 2. Hyperion simulated spectrum obtained from the PONMAC library without noise (dashed line) and with noise (solid line).

Figure 3. Set of five spectra obtained by resampling a simulated HyspIRI soil spectrum, derived from the PONMAC dataset, to bandwidths from 10 nm to 160 nm. The spectra were progressively offset with a factor of 0.1 for visualization purposes. Noisy bands in the water absorption ranges were removed.

Figure 4. Values of Variable Importance in Projection (VIP) in PLSR estimation models for clay (a–b), sand (c–d), silt (e–f) and SOC (g–h) using full spectrum data of PONMAC (left column) and LUCAS_C (right column) library. Predictors with VIP values greater than one (red area above the horizontal line in the plots) were considered significant for the PLSR models.

Figure 5. Ratio of performance to deviation (RPD) of clay, sand, silt and SOC estimation, obtained from the degradation of the spectral resolution of ***resampled*** spectra from 10 to 20, 40, 80 and 160 nm bandwidth.

Figure 6. Ratio of performance to deviation (RPD) of clay, sand, silt and SOC estimation, obtained from the degradation of the spectral resolution of ***simulated*** spectra from 10 to 20, 40, 80 and 160 nm bandwidth.

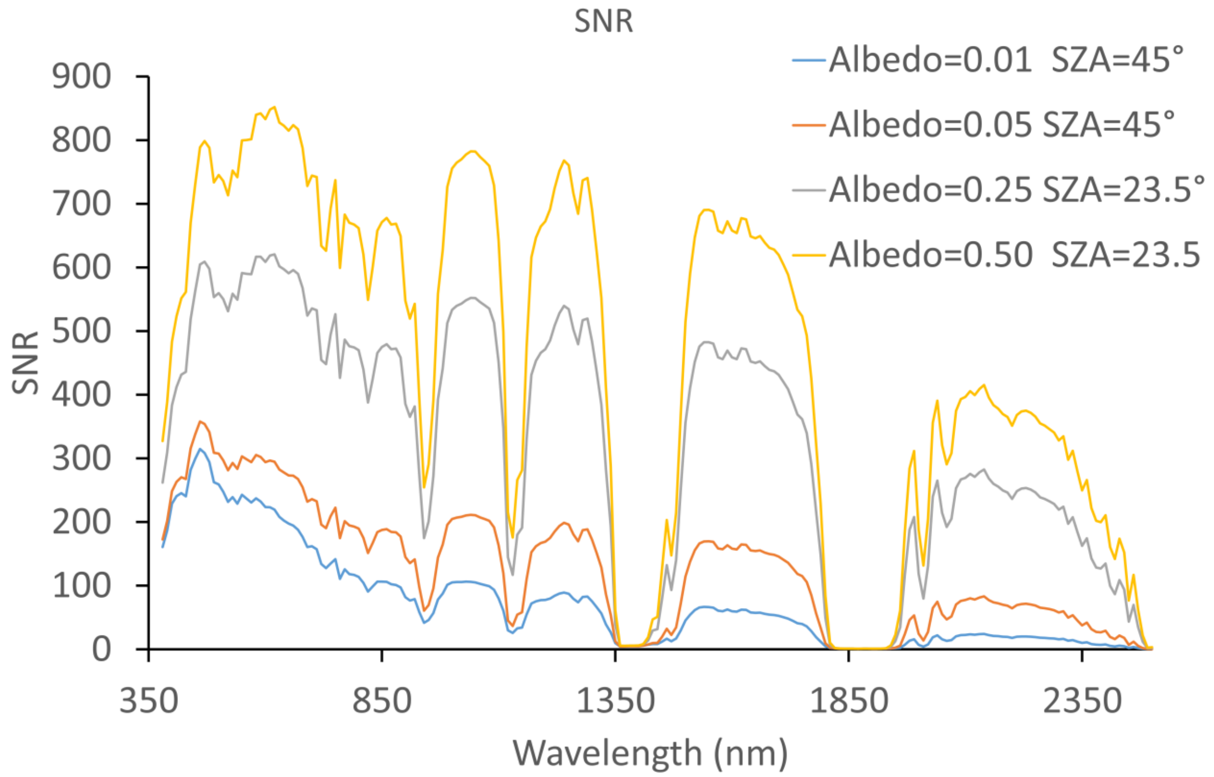

SNR
Albedo=0.01 SZA=45°
Albedo=0.05 SZA=45°
Albedo=0.25 SZA=23.5°
Albedo=0.50 SZA=23.5
SNR
0
100
200
300
400
500
600
700
800
900
350
850
1350
1850
2350
Wavelength (nm)

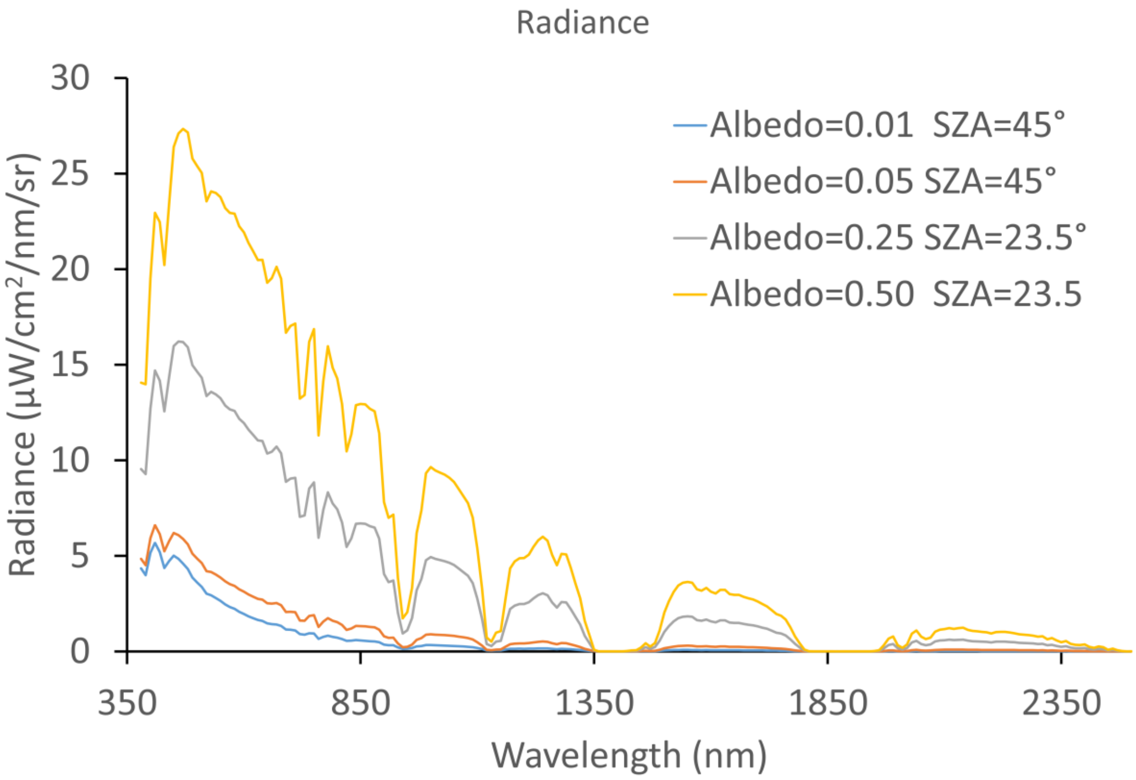

Radiance
Albedo=0.01 SZA=45°
Albedo=0.05 SZA=45°
Albedo=0.25 SZA=23.5°
Albedo=0.50 SZA=23.5
Radiance (µW/cm²/nm/sr)
0
5
10
15
20
25
30
350
850
1350
1850
2350
Wavelength (nm)

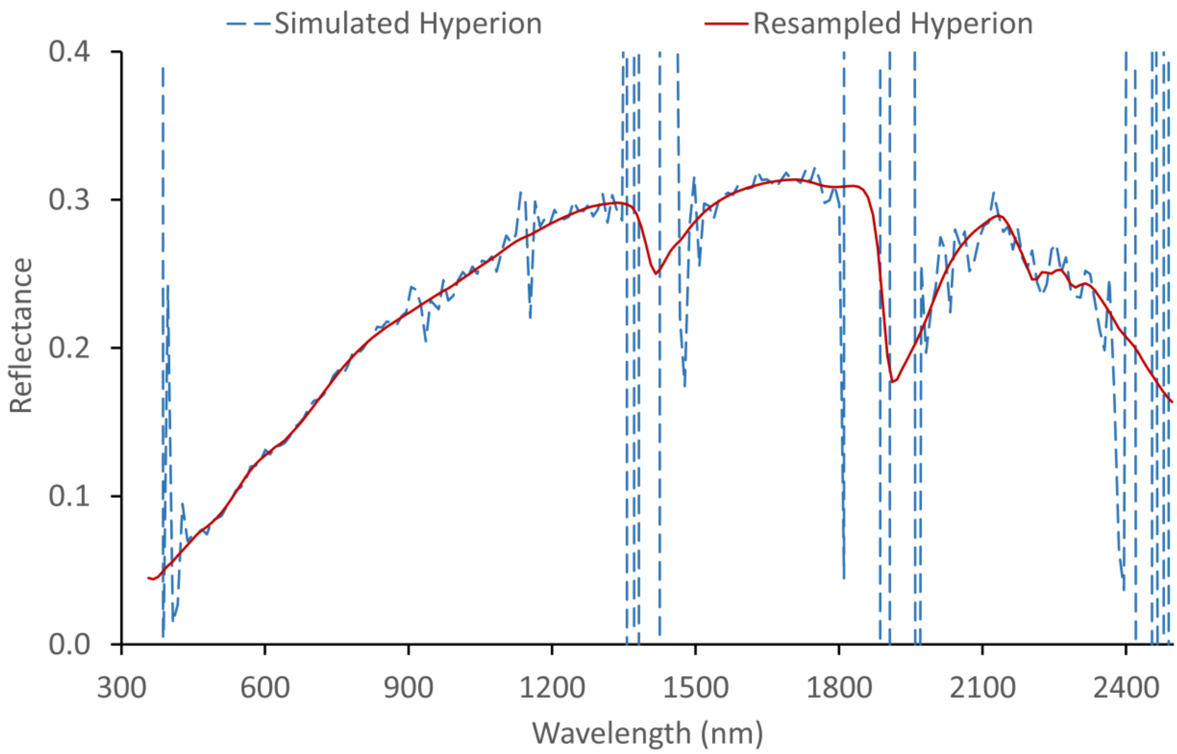
Simulated Hyperion
Resampled Hyperion
0.4
0.3
0.2
0.1
0.0
Reflectance
300
600
900
1200
1500
1800
2100
2400
Wavelength (nm)

799

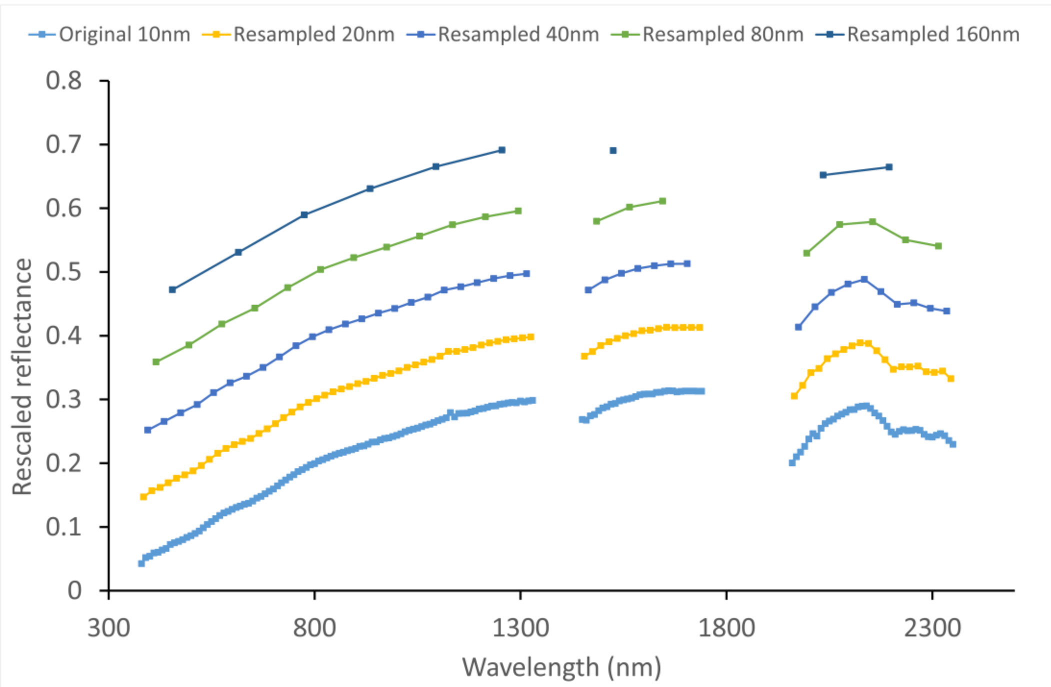
Original 10nm
Resampled 20nm
Resampled 40nm
Resampled 80nm
Resampled 160nm
0.8
0.7
0.6
0.5
0.4
0.3
0.2
0.1
0
Rescaled reflectance
300
800
1300
1800
2300
Wavelength (nm)

800

801

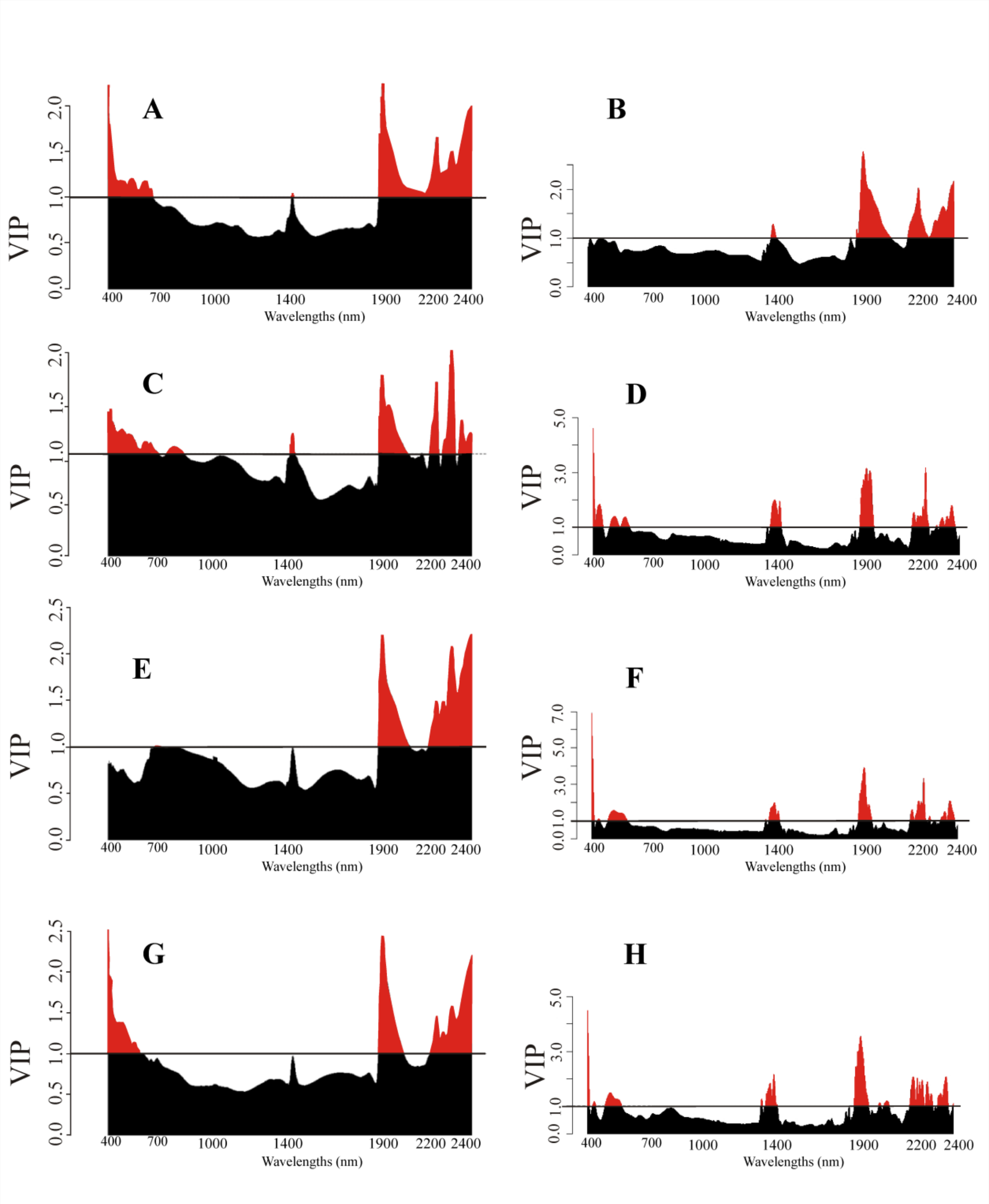

A
B
C
D
E
F
G
H
VIP
Wavelengths (nm)
400 700 1000 1400 1900 2200 2400

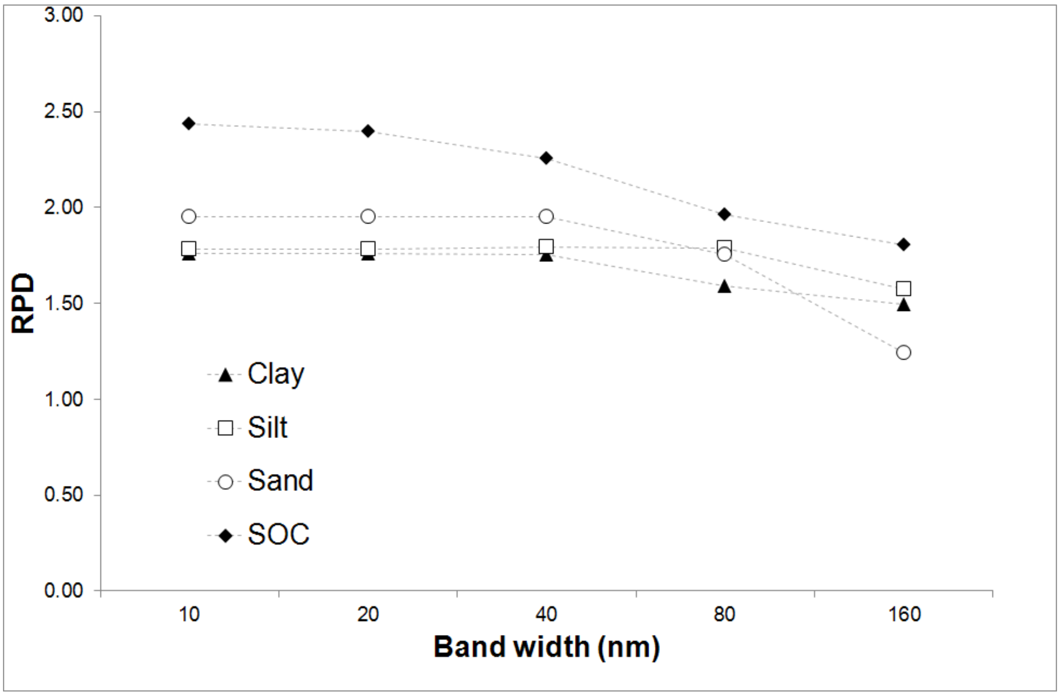
3.00
2.50
2.00
1.50
1.00
0.50
0.00
RPD
Clay
Silt
Sand
SOC
10
20
40
80
160
Band width (nm)

802

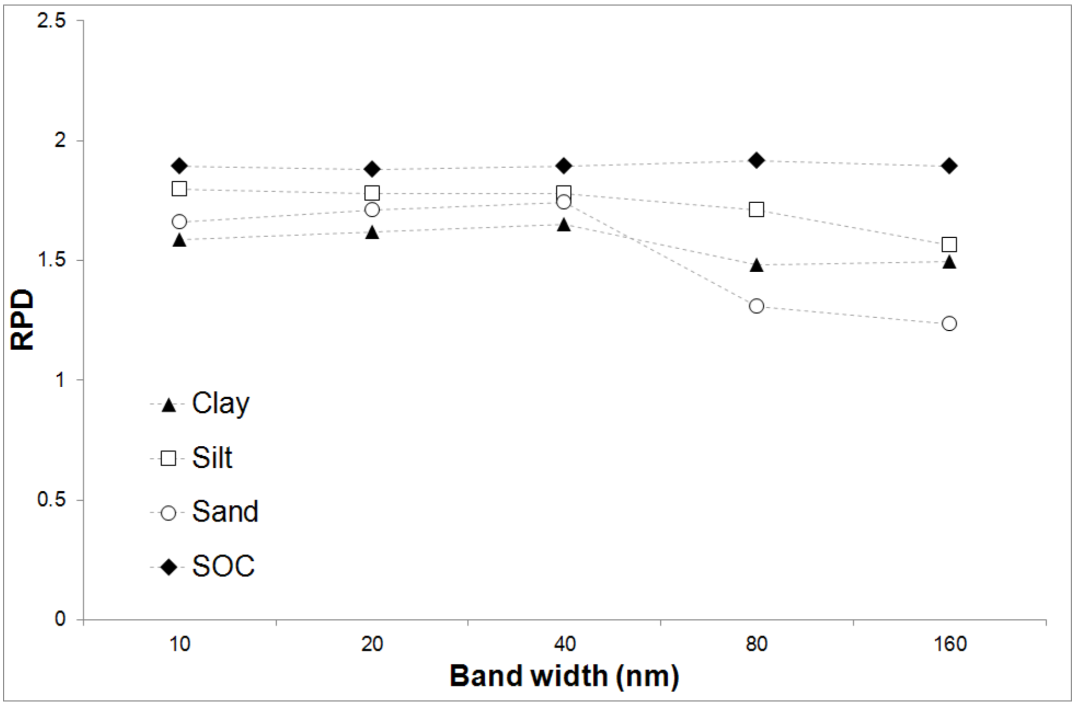
2.5
2
1.5
1
0.5
0
RPD
Clay
Silt
Sand
SOC
10
20
40
80
160
Band width (nm)

803

804

Table 1: Descriptive statistics of soil variables (clay, sand, silt and SOC) of the LUCAS_C and PONMAC datasets. Columns report basic statistics including the number of samples (n), standard deviation (sd), coefficient of variation (CV), as well as the type of data transformation eventually used.

Table 2: Main technical characteristics of the multispectral imagers considered in this study. The FWHM column reports the minimum and the maximum of the imager bandwidths. The SNR column reports the signal to noise ratio values and the wavelength at which it was calculated. The SNR condition column reports the radiance values under which the SNR were calculated.

Imager	Spectral bands	Spectral range	FWHM (nm)	SNR	SNR condition
EO-1 ALI	7	4 VNIR 3 SWIR	20-200	572 @550 nm 1040 @1550 nm 912 @2080 nm	17,08 mW/cm^2 sr µm 2,15 mW/cm^2 sr µm 0,68 mW/cm^2 sr µm
LANDSAT 8 OLI	7	5 VNIR 2 SWIR	20-200	100 @562 nm 100 @1610 nm 100 @2200 nm	30 W/m^2 sr µm 4,0 W/m^2 sr µm 1,7 W/m^2 sr µm
Sentinel-2 MSI	12	9 VNIR 3 SWIR	10-60	168 @560 nm 100 @1610 nm 100 @2190 nm	128 W/m^2 sr µm 4,0 W/m^2 sr µm 1,5 W/m^2 sr µm

Table 3: Main technical characteristics of the hyperspectral imagers considered in this study. The SNR column reports the signal to noise ratio values and the wavelength at which it was calculated. The SNR condition column reports the illumination condition used for the SNR calculation.

Imager	Spectral bands	Spectral range (nm)	FWHM (nm)	SNR	SNR condition
Hyperion	220	400-2500	10	161 @550 nm 147 @700 nm 110 @1125 nm 40 @2125 nm	nadir looking 60° sun-zenith angle 0.3 earth albedo
EnMAP	242	420-2450	10	> 500 @495 nm > 150 @2200 nm	nadir looking 30° sun-zenith angle 0.3 earth albedo
PRISMA	247	400-2500	7÷11	600 @ 0.65 µm > 400 @ 1.55 µm > 200 @ 2.1 µm	nadir looking 30° sun-zenith angle 0.3 earth albedo
HyspIRI	214	380-2510	10	560 @500 nm 356 @1500nm 236 @2200 nm	nadir looking 23,5° sun-zenith angle 0.25 earth albedo

Table 4: Noisy bands falling into the atmospheric gases absorption ranges that were removed before processing.

Imager	Wavelengths (nm)
Hyperion	356-397; 1134; 1356-1477; 1810-1971; 2405-2577
HyspIRI	380-390; 1360-1420; 1820-1950; 2410-2500
EnMAP	1346-1464; 1813-1951; 2408-2438
PRISMA	1352-1428; 1806-1955; 2403-2500
Landsat 8	1370
ALI	none
Sentinel-2	none

Table 5: Noise-free results obtained from PONMAC spectral library (***full spectrum*** and ***resampled*** datasets). Mean values of the multiple jack-knifing validation results of soil texture and SOC estimation models. The statistics used are: RMSE = Root Mean Square Error; RPD = Ratio of the Performance to Deviation; RPIQ = Ratio of Performance to Interquartile Range and coefficient of determination (R^2). Different letters within the LSD (least significant

difference) column denote a significant difference (P < 0.05) among RPIQ values according to Fisher's LSD’s test.

Variable	Resampling type	Spectra transformation[a]	PLSR components	RMSE (%)	RPD	RPIQ	R^2	LSD
Clay	Full spectrum	A+SG	10	4.82	1.97	3.07	0.71	a
	Hyperion	None	11	5.95	1.62	2.42	0.58	c
	HyspIRI	None	12	6.02	1.62	2.43	0.56	bc
	EnMAP	None	11	6.11	1.59	2.39	0.56	c
	PRISMA	None	12	5.91	1.64	2.43	0.58	bc
	Landsat 8	None	5	6.97	1.38	2.07	0.43	e
	ALI	None	7	6.40	1.50	2.25	0.52	d
	Sentinel-2	None	8	5.72	1.70	2.54	0.61	b
Sand	Full spectrum	None	12	5.38	1.83	2.51	0.69	ab
	Hyperion	None	12	5.36	1.86	2.55	0.67	a
	HyspIRI	A	11	5.54	1.79	2.45	0.66	b
	EnMAP	None	12	5.27	1.87	2.56	0.69	a
	PRISMA	None	13	5.43	1.82	2.50	0.67	ab
	Landsat 8	A	6	8.60	1.15	1.56	0.17	e
	ALI	A	8	7.15	1.38	1.88	0.44	d
	Sentinel-2	None	9	5.96	1.66	2.28	0.60	c
Silt	Full spectrum	None	8	4.77	1.95	3.17	0.71	a
	Hyperion	A+SG	8	5.35	1.72	2.77	0.64	c
	HyspIRI	A+SG+D	7	5.11	1.83	2.95	0.66	b
	EnMAP	A	8	5.08	1.82	2.97	0.66	b
	PRISMA	A+SG+D	6	5.08	1.82	2.95	0.67	b
	Landsat 8	A	6	5.87	1.56	2.54	0.55	e
	ALI	A	7	5.60	1.64	2.69	0.60	cd
	Sentinel-2	A	7	5.82	1.58	2.56	0.58	de
SOC	Full spectrum	A+SG	13	0.20	1.78	3.12	0.65	a
	Hyperion	A+SG	19	0.22	1.70	2.95	0.62	bc
	HyspIRI	None	12	0.22	1.65	2.86	0.60	c
	EnMAP	A+SG+D	13	0.20	1.80	3.11	0.67	a
	PRISMA	A	14	0.21	1.75	3.02	0.65	ab
	Landsat 8	None	6	0.25	1.46	2.51	0.50	e
	ALI	None	8	0.25	1.43	2.46	0.49	e
	Sentinel-2	A	7	0.23	1.55	2.68	0.56	d

[a] data were transformed using: absorbance (A), first derivative (D) and/or the Savitzky-Golay (SG) smoothing filter

Table 6: Noise-free results obtained from LUCAS_C spectral library (***full spectrum*** and ***resampled*** datasets). Mean values of the multiple jack-knifing validation results of soil texture

and SOC estimation models. The statistics used are: RMSE = Root Mean Square Error; RPD = Ratio of the Performance to Deviation; RPIQ = Ratio of Performance to Interquartile Range and coefficient of determination (R^2). Different letters within the LSD column denote a significant difference ($P < 0.05$) among RPIQ values according to Fisher's LSD's test.

Variable	Resampling type	Spectra transformation[a]	PLSR components	RMSE (%)	RPD	RPIQ	R^2	LSD
Clay	Full spectrum	A	18	7.63	1.69	2.34	0.64	bc
	Hyperion	A	16	7.98	1.62	2.29	0.61	c
	HyspIRI	A	18	7.71	1.68	2.38	0.64	b
	EnMAP	A+SG+D	18	7.39	1.75	2.48	0.66	a
	PRISMA	A+SG+D	18	7.78	1.66	2.34	0.63	b
	Landsat 8	A	3	10.10	1.27	1.81	0.38	d
	ALI	A	9	9.87	1.30	1.85	0.40	d
	Sentinel-2	A	6	9.92	1.30	1.84	0.40	d
Sand	Full spectrum	A+SG+D	12	12.88	1.25	1.78	0.37	ab
	Hyperion	A	15	13.35	1.22	1.73	0.32	c
	HyspIRI	A	17	12.93	1.25	1.79	0.37	a
	EnMAP	A+SG+D	17	13.28	1.22	1.75	0.30	bc
	PRISMA	A	17	12.98	1.24	1.78	0.35	ab
	Landsat 8	None	7	15.05	1.07	1.53	0.12	e
	ALI	A	9	14.58	1.10	1.59	0.17	d
	Sentinel-2	A	7	14.58	1.11	1.59	0.16	d
Silt	Full spectrum	A+SG+D	14	11.42	1.22	1.74	0.31	cd
	Hyperion	A+SG+D	18	10.93	1.26	1.81	0.38	b
	HyspIRI	A	18	10.66	1.30	1.85	0.40	a
	EnMAP	A	18	10.63	1.31	1.87	0.39	a
	PRISMA	A	18	10.75	1.29	1.84	0.39	ab
	Landsat 8	A	7	11.66	1.19	1.70	0.28	e
	ALI	A	9	11.27	1.23	1.76	0.33	c
	Sentinel-2	A	7	11.61	1.20	1.71	0.28	de
SOC	Full spectrum	A+SG+D	17	0.42	1.35	1.75	0.42	ab
	Hyperion	A	14	0.46	1.23	1.59	0.27	c
	HyspIRI	A	18	0.41	1.37	1.79	0.44	a
	EnMAP	A+SG+D	18	0.41	1.38	1.79	0.45	a
	PRISMA	A+SG+D	18	0.42	1.33	1.73	0.42	b
	Landsat 8	A	5	0.51	1.09	1.40	0.16	e
	ALI	A	5	0.51	1.09	1.41	0.16	e
	Sentinel-2	A	7	0.50	1.13	1.46	0.20	d

[a] data were transformed using: absorbance (A), first derivative (D) and/or the Savitzky-Golay (SG) smoothing filter

Table 7: Results obtained from PONMAC spectral library with the addition of noise and atmospheric effects (***simulated*** datasets). Mean values of the multiple jack-knifing validation results of soil texture and SOC estimation model. The statistics used are: RMSE = Root Mean

Square Error; RPD = Ratio of the Performance to Deviation; RPIQ = Ratio of Performance to Interquartile Range and coefficient of determination (R^2). Different letters within the LSD column denote a significant difference ($P < 0.05$) among RPIQ values according to Fisher's LSD's test.

Variable	Resampling type	Spectra transformation[a]	PLSR components	RMSE (%)	RPD	RPIQ	R^2	LSD
Clay	Hyperion	SG	6	7.34	1.31	1.98	0.39	e
	HyspIRI	None	9	6.73	1.43	2.16	0.47	b
	EnMAP	A+SG+D	6	6.12	1.57	2.35	0.57	a
	PRISMA	None	8	6.24	1.54	2.33	0.54	a
	Landsat 8	None	5	6.93	1.38	2.07	0.45	cd
	ALI	None	8	6.58	1.45	2.15	0.51	bc
	Sentinel-2	None	5	7.08	1.35	2.03	0.42	de
Sand	Hyperion	SG	9	8.46	1.17	1.59	0.20	d
	HyspIRI	None	12	6.45	1.52	2.10	0.53	b
	EnMAP	A+SG	12	6.17	1.60	2.17	0.57	a
	PRISMA	A+SG	12	6.23	1.58	2.17	0.57	a
	Landsat 8	A	6	9.06	1.08	1.48	0.11	e
	ALI	A	8	7.83	1.25	1.73	0.32	c
	Sentinel-2	None	5	8.79	1.12	1.55	0.13	d
Silt	Hyperion	SG	7	6.53	1.40	2.27	0.46	d
	HyspIRI	A+SG	8	5.29	1.73	2.80	0.65	a
	EnMAP	A+SG	8	5.23	1.76	2.85	0.65	a
	PRISMA	A+SG	8	5.40	1.70	2.77	0.63	a
	Landsat 8	A	4	6.16	1.47	2.39	0.53	bc
	ALI	A	8	6.06	1.51	2.44	0.53	b
	Sentinel-2	None	4	6.42	1.43	2.34	0.46	cd
SOC	Hyperion	A+SG	7	0.28	1.30	2.25	0.39	c
	HyspIRI	A+SG	12	0.25	1.44	2.49	0.49	a
	EnMAP	None	6	0.25	1.45	2.51	0.50	a
	PRISMA	A+SG	7	0.25	1.45	2.48	0.51	a
	Landsat 8	None	6	0.25	1.44	2.48	0.49	a
	ALI	None	7	0.26	1.37	2.38	0.44	b
	Sentinel-2	None	3	0.29	1.26	2.17	0.36	c

[a] data were transformed using: absorbance (A), first derivative (D) and/or the Savitzky-Golay (SG) smoothing filter

Table 8: Results obtained from LUCAS_C spectral library with the addition of noise and atmospheric effects (***simulated*** datasets). Mean values of the multiple jack-knifing validation results of soil texture and SOC estimation models. The statistics used are: RMSE = Root Mean Square Error; RPD = Ratio of the Performance to Deviation; RPIQ = Ratio of Performance to Interquartile Range and coefficient of determination (R^2). Different letters within the LSD column denote a significant difference ($P < 0.05$) among RPIQ values according to Fisher's LSD's test.

Variable	Resampling type	Spectra transformation[a]	PLSR components	RMSE (%)	RPD	RPIQ	R^2	LSD
Clay	Hyperion	SG+D	7	16.98	0.90	1.27	-1.56[rc2]	c
	HyspIRI	A	10	9.14	1.41	2.00	0.49	a
	EnMAP	A+SG	11	9.33	1.38	1.95	0.46	a
	PRISMA	A+SG	7	9.11	1.41	2.00	0.50	a
	Landsat 8	A	5	10.11	1.28	1.81	0.37	b
	ALI	A	8	10.09	1.27	1.80	0.37	b
	Sentinel-2	A	6	10.25	1.26	1.78	0.36	b
Sand	Hyperion	SG+D	4	17.92	0.95	1.37	-0.44	e
	HyspIRI	A	11	14.53	1.11	1.59	0.17	a
	EnMAP	A+SG	12	14.57	1.11	1.59	0.17	ab
	PRISMA	A+SG	7	14.50	1.11	1.59	0.18	ab
	Landsat 8	A	5	15.25	1.06	1.51	0.10	d
	ALI	A	8	14.87	1.09	1.55	0.13	bc
	Sentinel-2	A	3	15.18	1.06	1.52	0.10	cd
Silt	Hyperion	A	5	14.71	0.96	1.37	-0.19	c
	HyspIRI	A	8	11.67	1.19	1.69	0.28	ab
	EnMAP	A+SG	9	11.59	1.20	1.71	0.29	ab
	PRISMA	A+SG	7	11.48	1.21	1.72	0.30	a
	Landsat 8	A	7	11.73	1.18	1.68	0.27	b
	ALI	A	8	11.59	1.20	1.71	0.29	ab
	Sentinel-2	A	4	11.90	1.16	1.67	0.25	b
SOC	Hyperion	SG+D	7	0.53	1.05	1.36	0.06	d
	HyspIRI	A	12	0.48	1.15	1.48	0.23	b
	EnMAP	A+SG+D	9	0.48	1.17	1.51	0.25	ab
	PRISMA	A+SG	7	0.48	1.17	1.52	0.26	a
	Landsat 8	A	7	0.51	1.09	1.40	0.14	c
	ALI	A	7	0.51	1.09	1.41	0.15	c
	Sentinel-2	A	6	0.51	1.09	1.41	0.13	c

[a] data were transformed using: absorbance (A), first derivative (D) and/or the Savitzky-Golay (SG) smoothing filter

Table 9: Number of bands and signal to noise ratio (SNR) of HispIRI, PRISMA and EnMAP imagers in two spectral ranges (400 ÷ 600 nm and 2000 ÷ 2400 nm).

Spectral range	Imager	Bands (n.)	SNR mean	SNR st.dev.
400 -600 nm	HyspIRI	21	546.25	71.10
	PRISMA	25	438.34	107.51
	EnMap	35	536.57	50.19
2000 - 2400 nm	HyspIRI	41	218.27	52.49
	PRISMA	52	166.37	48.98
	EnMap	48	146.08	41.64